Materials Advances

ROYAL SOCIETY OF CHEMISTRY

PAPER

View Article Online
View Journal | View Issue

Cite this: *Mater. Adv.*, 2024, 5, 6910

Intravesical cascade delivery of active monoterpene coumarin for bladder cancer therapy†

Yanwei Lai,‡[a] Dashi Deng,‡[ab] Simin Yuan,[b] Xiaocen Liu,[c] Qifang Lei*[c] and Guangzhi Li *[ab]

Albumin proteins have been extensively explored for functionalized delivery of therapeutics. However, their potential in intravesical delivery has not been thoroughly investigated. In this work, we developed a green method for the synthesis of albumin nanocarriers that can efficiently encapsulate the active monoterpene coumarin UM-15 and assemble with fluorinated chitosan (FCS) to form UM-15@BSA/FCS nanoparticles (NPs). Upon intravesical perfusion, BSA/FCS NPs serving as the nano-vehicles of UM-15 demonstrate exceptional transepithelial delivery, efficient intratumoral diffusion, and high tumor-targeting uptake capacities. These remarkable advantages can be attributed to their notable cascade delivery performances, which involve FCS-driven rearrangement of bladder epithelium tight junctions and the charge reversal effect-induced dissociation behavior of FCS-albumin complexes, as well as the high tumor selectivity mediated by albumin-binding protein (SPARC) and disulfide bonds. Additionally, UM-15 loaded in those nanovehicles demonstrates significant induction of apoptosis and stemness suppression of bladder cancer cells. With above effects acting synergistically, remarkably improved intravesical treatment outcomes are achieved in both mouse orthotopic and patient-derived orthotopic xenograft models, with reduced toxic side effects. Thus, our study introduces a novel therapeutic agent for BCa therapy and presents a promising avenue for the tumor targeted delivery of therapeutics through an intravesical cascade delivery mechanism.

Received 23rd May 2024,
Accepted 18th July 2024

DOI: 10.1039/d4ma00528g

rsc.li/materials-advances

Introduction

Bladder cancer (BCa), characterized by a substantial recurrence (50–70%) and progression rate (10–30%), imposes significant financial and psychological burdens on patients due to the necessity of lifelong follow-up care and frequent treatment expenses.[1,2] Intravesical therapy, as a crucial adjunctive strategy following transurethral resection, plays an essential role in eliminating residual tumor cells to mitigate the risk of BCa recurrence or progression.[3,4] To date, conventional chemotherapeutic drugs (*e.g.* mitomycin, epirubicin, or gemcitabine), and Bacillus Calmette-Guérin (BCG) are still the first-line agents for intravesical treatment of BCa.[5] However, the limited bioavailability of perfusion drugs due to the epithelial barrier and the treatment resistance triggered by stem-like BCa cells dramatically attenuate the instillation therapy efficacy. Additionally, the subsequently high-dose multiple intravesical therapy tends to cause serious adverse effects and chemoresistance.[6,7] Consequently, there is growing interest in investigating novel therapeutic drugs and efficient drug delivery strategies to improve the BCa treatment.

UM-15, a newly discovered monoterpene coumarin compound derived from *Ferula sinkiangensis*, exhibits potent cytotoxic activities against several bladder cancer cell lines and effectively suppresses the stem maintenance of BCa stem-like cells, demonstrating significant advantages of UM-15 as an alternative chemotherapeutic for BCa therapy. However, UM-15 is a hydrophobic component and shows potent splenorenal toxicity of non-tumor selectivity. Besides, the bladder epithelial barrier is also a challenge for the intravesical delivery of perfusion therapeutics. These drawbacks hinder the potential of free UM-15 for tumor-targeted transepithelial penetration, significantly limiting its therapeutic application in intravesical instillation of BCa. In light of this predicament, we herein

[a] *Luohu Clinical College of Shantou University Medical College, Shantou University Medical College, Shantou, 515000 Guangdong, China. E-mail: guangzhili@email.szu.edu.cn*
[b] *Institute of Urology, The Affiliated Luohu Hospital of Shenzhen University, Shenzhen University, Shenzhen 518000, China*
[c] *Institute of Urology, South China Hospital, Health Science Center, Shenzhen University, Shenzhen 518116, China. E-mail: leiqifang66@163.com*

† Electronic supplementary information (ESI) available. See DOI: https://doi.org/10.1039/d4ma00528g

‡ Y. L. and D. D. contributed equally and are co-first authors for this work.

attempt to develop a well-suited perfusion formulation that can serve as an effective drug carrier for UM-15 to enable efficient transepithelial tumor-targeted delivery.

Albumin, an important functional serum protein, plays an increasing role as a versatile carrier in controlled delivery applications.[8,9] Meanwhile, its binding proteins such as SPARC and gp60 overexpressed in some tumor tissues have been explored in recent years to serve as a specific transporter for albumin loading drugs.[10–12] It has been discovered that SPARC is overexpressed in cancerous bladder epithelium and closely associated with the progression and metastasis of BCa.[13,14] Nonetheless, little is known about SPARC as targeting receptors on intravesical drug delivery, and indeed, albumin-based delivery applications for bladder perfusion have been scarcely investigated. Hence, we herein designed a straightforward, convenient, and cost-effective method to fabricate UM-15 loading albumin nanostructures (UM-15@BSA).

Recently, fluorinated polymers such as fluorinated polyethylenimines (PEIs) and dendrimers have been reported to have promising potential in protein/peptide delivery.[15–17] These fluoroamphiphiles could not only be fabricated into nanoparticles with biomacromolecules *via* the co-assembly performance, but can also improve the affinity of materials to cell membranes and facilitate the effective cellular uptake of loading agents.[18] Overall, the ''fluorination effect'' offers fluorinated polymers significant advantages over non-fluorinated alternatives in terms of nanocomplex fabrication, cytotoxicity, protein/peptide denaturation, and cellular uptake, as well as tissue penetration.[19–21] All along, our research studies have been focused on the transepithelial delivery of macromolecular protein drugs, which have fully confirmed that fluorinated chitosan (FCS) demonstrates a more highly efficient transepithelial delivery and better intravesical biosafety compared with its non-fluorinated alternatives (CS), and is an ideal vehicle for the intravesical delivery of protein drugs. Thus, building upon our previous reports, here we further coated the aforementioned albumin particles with FCS to facilitate its intravesical application.[22–24]

In our study, BSA mixing with UM-15 under a thermal annealing operation could form UM-15@BSA nanostructures by the hydrogen bonding or van der Waals forces-mediated assembly of BSA. As the negative surface potential, UM-15@BSA would further assemble with positive FCS to form UM-15@BSA/FCS NPs *via* electrostatic interaction. Interestingly, the UM-15@BSA/FCS NPs demonstrated a notable capacity for transepithelial delivery driven by tight junction regulation, as well as efficient permeability within tumor tissues, due to their charge reversal-dependent dissociation behavior in a microacidic environment. In addition, the naked BSA platform entering into tumor tissue showed remarkably enhanced tumor uptake efficacy *via* the albumin-binding protein (SPARC) pathway, along with outstanding tumor microenvironment-responsive drug release, which is able to achieve efficient tumor-targeting delivery of its loading agents. In summary, the BSA/FCS NPs function as nano-vehicles for the targeted transportation of UM-15 from the bladder lumen to the tumor cells *via* a cascade pushing mechanism. Furthermore, UM-15 loaded in the carriers, not only is proven to be an effective chemotherapeutic agent against bladder cancer cells, but also possesses the ability to hinder the stem maintenance in BCa stem-like cells, thereby offering potential solutions to the current dilemma in BCa treatment (Scheme 1). With the above advantages acting collectively, impressive *in vivo* therapeutic effects are achieved by applying such UM-15@BSA/FCS NPs for intravesical treatment in both mouse orthotopic and PDOX BCa models. Thus, this work presents a new monoterpene coumarin compound as a potential therapeutic agent for BCa and proposes a facile approach to develop albumin-based instillation platforms for its transepithelial tumor-targeted delivery *via* a cascade delivery mechanism.

Results and discussion

The preparation of UM-15@BSA/FCS NPs was commenced with the synthesis of UM-15 (ESI,† Scheme S1), which was initially isolated from *F. sinkiangensis* and identified as a potential therapeutic candidate for BCa.[25] According to the spectroscopy analysis (Fig. S1, ESI†), the monoterpene coumarin structure of UM-15 was established. Subsequently, albumin perfusion nano-systems loaded with UM-15 were synthesized using co-assembly strategies. As shown in Fig. 1a, BSA was mixed with UM-15 under a mild thermal annealing operation ($\sim$70 °C) to form UM-15@BSA *via* the hydrogen bonding or van der Waals force-mediated assembly of BSA. Then, FCS, a highly effective intravesical carrier synthesized through the fluorinated modification of chitosan, was added at various weight ratios (1 : 4–2 : 1) to assemble with UM-15@BSA forming smart self-assembled UM-15@ BSA/FCS NPs. As the control, unloaded BSA/FCS NPs were prepared following the same methodology.

The UV-visible absorption spectra of different UM-15 loading formulations were recorded (Fig. 1b). As expected, the UM-15 characteristic absorption at $\sim$330 nm was observed in that of UM-15-encapsulated nano-platforms. In order to identify the interaction of UM-15 with BSA, circular dichroism (CD) spectroscopy and isothermal titration calorimetry (ITC) were employed. As shown in Fig. S2a (ESI†), with the addition of UM-15, the negative Cotton effect of BSA at 208 nm and 220 nm was significantly reduced indicating the decrease of the α-helix structure in BAS, which suggested that the combination of UM-15 and BSA led to the conformational change of BSA. Besides, according to the correlation between thermodynamic parameters and interaction types, $\Delta H = -1.539 \times 10^4$ cal mol^{-1} and $\Delta S = -52.1$ cal mol^{-1} deg^{-1} demonstrated that the main binding force between UM-15 and BSA is the weak interaction force such as the hydrogen bond or van der Waals force (Fig. S2b, ESI†). The size distribution and zeta potential of the obtained UM-15@BSA and UM-15@ BSA/FCS NPs prepared at varied UM-15@BSA:FCS weight ratios were measured. The results showed that compared to UM-15@BSA complexes that exhibited a hydrodynamic size at 142 $\pm$ 15 nm with a negative charge (−18.1 $\pm$ 2.1 mV), UM-15@BSA/FCS NPs prepared at a

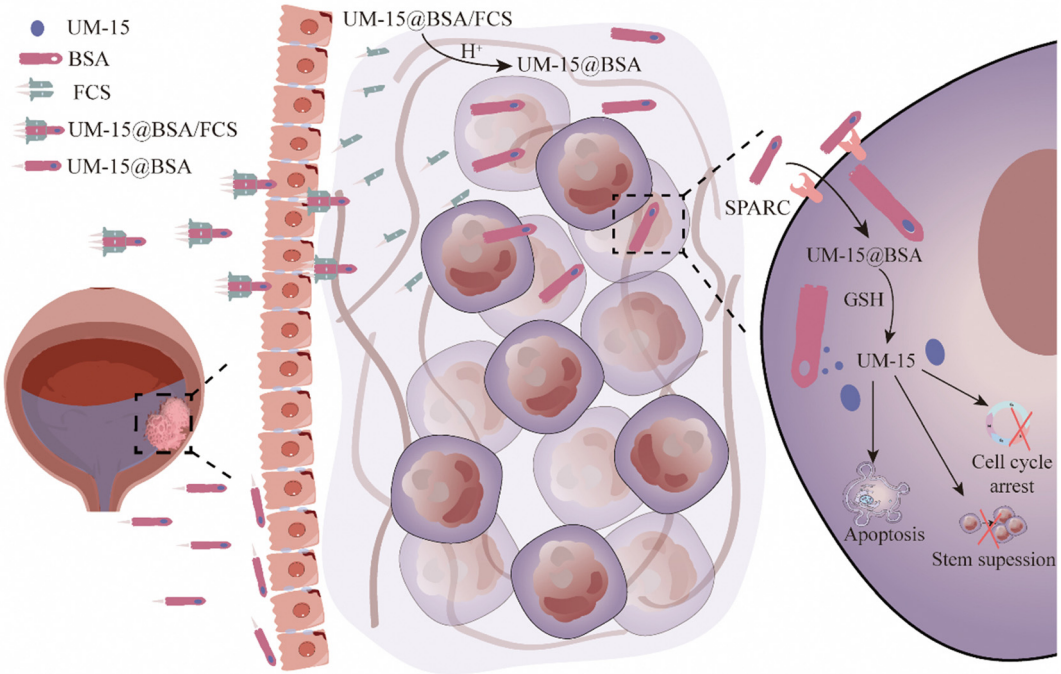

Scheme 1 UM-15@BSA/FCS NPs, a novel therapeutic agent for BCa therapy and presents a promising avenue for the tumor targeted delivery of therapeutics though an intravesically cascade delivery mechanism.

weight ratio of 1 : 1 demonstrated obviously larger hydrodynamic diameters (230 ± 21 nm) with the narrowest size distribution, as well as a remarkable positive zeta potential (17.8 ± 5.6 mV) (Fig. 1c and d). The DL of UM-15 in UM-15@BSA was calculated to be 18.9 ± 2.0% and the EE was found to be 86.3 ± 5.7%. Finally, the freeze-drying stability of these nano-agents was examined through the analysis of the polydispersity index (PDI). As shown in Fig. 1e, UM-15@BSA formulations showed no remarkable fluctuations in the PDI, indicating the conspicuous freeze-drying stability of UM-15@BSA-based nanostructures. Thus, the above results provide evidence for the successful construction of UM-15 loading formulations.

Considering disulfide bonds are the intrinsic structure of albumin, we supposed that the UM-15@BSA/FCS NPs might exhibit pH-sensitive and reduction-responsive properties. Then, we detected the charge inversion, size distribution, morphology change, and drug release profile under conditions that mimic the tumor microenvironment with a low pH and high GSH. As shown in Fig. 1f, the DLS data displayed a sensitively zeta-potential inversion of UM-15@BSA from −18.1 ± 2.1 mV to 27.8 ± 5.6 mV as the solution gradually became more acidic. Besides, consecutive changes in size-distributions transitioning from a single narrow peak to the tanglesome distributions were also observed (Fig. 1g). These phenomena suggest the shedding of FCS from UM-15@BSA/FCS NPs, triggered by the aforementioned charge-inversion mechanism, as well as the disintegration of bare UM-15@BSA through GSH-dependent disulfide bond breakage. Furthermore, the obtained UM-15@BSA/FCS NPs with a uniform spherical structure also showed noticeable morphology changes after incubation in PBS (pH 5.5, 5 mM GSH) for 24 h as revealed by transmission electron microscopy (TEM) imaging (Fig. 1h), further confirming the cascade disintegration capacity of UM-15@BSA/FCS NPs in response to a low pH value and high GSH. In terms of the *in vitro* release performance, it was found that 79.9 ± 1.9% of the UM-15 payload was released from the NPs within 120 h after incubation with 5 mM GSH in PBS (pH 6.5), which was significantly higher than the amount released at separate high GSH (59.6 ± 2.4%) or low pH stimulations (50.6 ± 1.3%). In contrast, the release ratio of UM-15 in PBS (pH = 7.4) did not exceed 20.6 ± 1.3%. These findings confirmed that UM-15@BSA/FCS NPs remain stable under physiological conditions and effectively release the payload in a simulated tumor microenvironment.[26–28]

The transepithelial delivery capacities of different BSA-based formulations were then assessed by an *in vivo* intravesical instillation experiment. Cy5.5 fluorescence dye labeled BSA ($BSA_{Cy5.5}$) was employed to prepare UM-15@$BSA_{Cy5.5}$ and UM-15@$BSA_{Cy5.5}$/FCS NPs following the aforementioned method. Mice with orthotropic MB49 bladder tumor were intravesically treated with free $BSA_{cy5.5}$, UM-15@$BSA_{cy5.5}$, or UM-15@$BSA_{cy5.5}$/FCS NPs at an equivalent $BSA_{cy5.5}$ dosage (1.0 mg mL^{-1}) for 1 h, and then their bladders were collected for confocal laser scanning microscopy (CLSM) analysis. As illustrated in Fig. 2a, a more pronounced and extensive distribution of Cy5.5 fluorescence was detected in the bladder tissues perfused with UM-15@$BSA_{cy5.5}$/FCS NPs. In contrast, bladders instilled with $BSA_{cy5.5}$ or UM-15@$BSA_{cy5.5}$ exhibited weak fluorescence or limited presence only at the boundary of the bladder epithelium. The semi-quantitative analysis of the fluorescence intensity (Fig. 2b) and penetration depth (Fig. 2c), based on

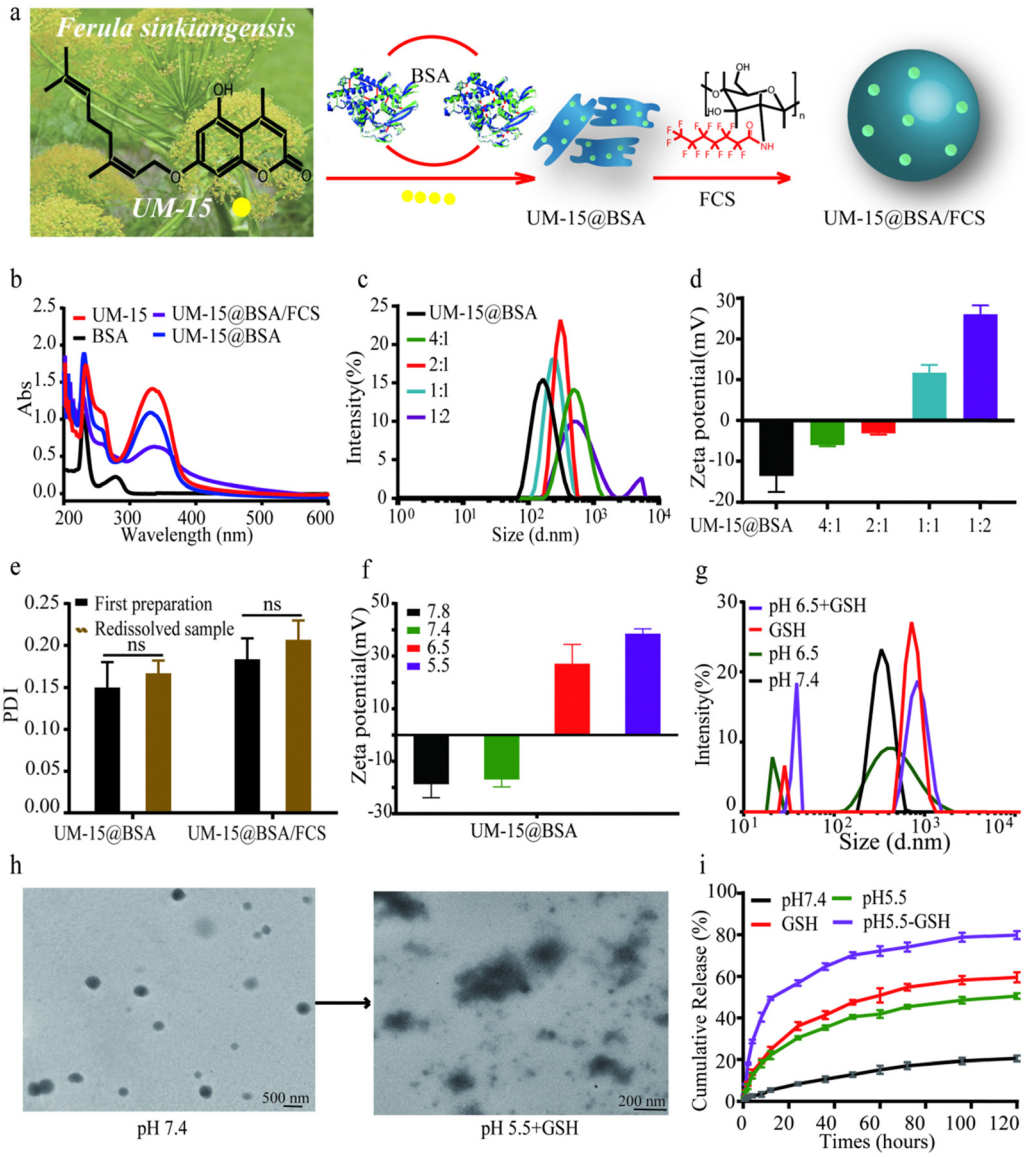

Fig. 1 Synthesis and characterization of UM-15@BSA/FCS NPs. (a) Schematic illustration of the preparation of UM-15@BSA/FCS NPs. (b) UV-visible absorbance of BSA, free UM-15, UM-15@BSA, and UM-15@ BSA/FCS nanoparticles. Hydrodynamic diameters (c) and zeta potentials (d) of UM-15@BSA and UM-15@BSA/FCS prepared at various feeding weight ratios measured by DLS. (e) Freeze-drying stability of UM-15@BSA-based nanostructures as determined by the fluctuation of the PDI and drug content. (f) The charge inversion effect indicated as the zeta potentials in different pH environments (5.5–7.8). The changes in the size distribution (g) and morphology (h) of UM-15@BSA/FCS NPs in response to low pH and high GSH were determined by DLS and TEM, respectively. (i) The *in vitro* release performance of UM-15@BSA/FCS under different conditions. ns, $p > 0.05$ analyzed using Student's *t* test. Data are presented as mean ± standard deviation.

the observations in Fig. 2a, further confirmed the enhanced transepithelial penetration capability of UM-15@BSA$_{cy5.5}$/FCS NPs due to their FCS coating.

Based on our previous research findings, it has been suggested that FCS has the potential to facilitate the efficient delivery of protein therapeutics across the bladder epithelium by regulating the tight junctions in a reversible manner.[22] Thus, in order to elucidate the possible mechanism of transepithelial absorption for UM-15@BSA/FCS NPs, an immunofluorescence staining assay was performed to evaluate the distribution of epithelial cell junction proteins in the bladder epithelium (SV-HUC-1). As shown in Fig. 2d, compared with the free BSA and UM-15@BSA groups, the continuous protein distribution pattern of several tight junction relative proteins (ZO-1, E-cadherin, and Occludin) along the bladder epithelium interfaces was distinctly destroyed after UM-15@BSA/FCS NP incubation. Additionally, the phosphorylation level of MLC (pMLC), which was closely associated with the management of the cell cytoskeletal structure, was also obviously up-regulated after UM-15@BSA/FCS NP treatment (Fig. 2e and f). Thus, the above results indicate that the binding of FCS could promote the phosphorylation of MLC, leading to the opening of tight

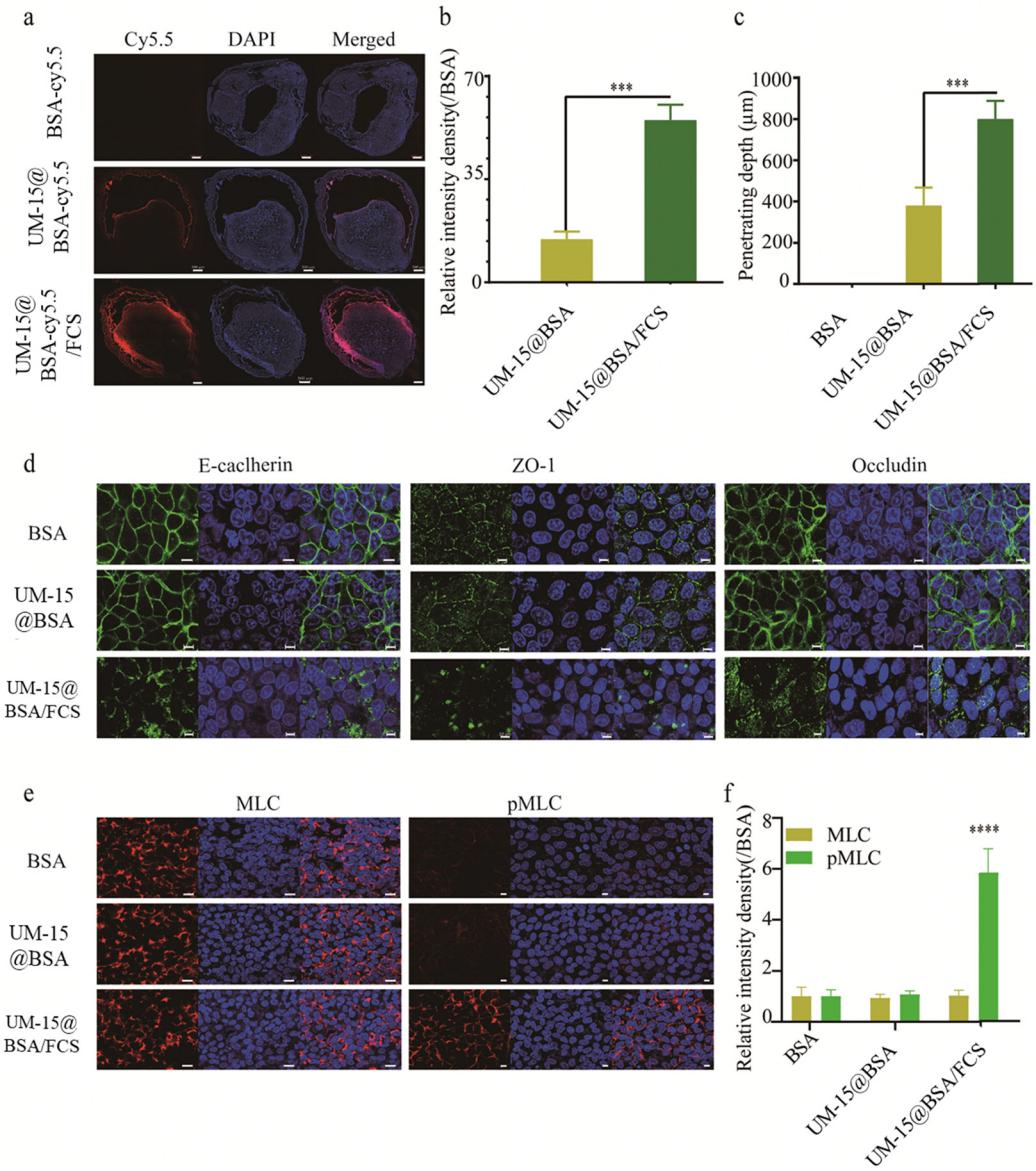

Fig. 2 Transepithelial penetration and potential mechanism of UM-15@BSA/FCS NPs. (a) Confocal images of cold-cup biopsy of orthotopic MB49 bladder tumors collected from mice instilled with different BSA-based formulations for 1 h (scale bar, 500 μm). Semiquantitative analysis of the fluorescence intensity (b) and penetration depth (c) of $BSA_{\text{-Cy5.5}}$ based on the observations in (a) using ImageJ software. (d) Immunofluorescence imaging to show the distribution of tight junction relative proteins, E-cadherin and ZO-1, occluding the cell boundary (scale bar 10 μm). (e) The protein expression and phosphorylation level of MLC (pMLC) in SV-HUC-1 cells treated with UM-15@BSA/FCS NPs (scale bar 10 μm). (f) Semiquantitative analysis of the fluorescence signal of MLC and pMLC observed in (e). ***$p < 0.001$ and ****$p < 0.0001$ analyzed using Student's t test. Data are presented as mean ± standard deviation.

junctions in the bladder epithelium and subsequently enhancing the delivery of encapsulated BSA therapeutics, which are all consistent with that reported in our previous research.[22] Furthermore, the reduction in size resulting from the shedding of FCS from UM-15@BSA/FCS NPs due to pH-responsive charge inversion, along with the enhanced permeability through tight junction regulations, collectively contribute to the remarkable intratumoral penetration capability of UM-15@BSA/FCS NPs.

Once the perfusion agents have successfully traversed the bladder epithelial barrier and entered the tumor tissue, the subsequent challenge lies in achieving effective uptake by the tumor cells. To assess the cellular uptake efficiency of various BSA-based agents, mouse bladder cancer MB49 cells were incubated with free $BSA_{\text{-Cy5.5}}$, UM-15@$BSA_{\text{-Cy5.5}}$, or UM-15@$BSA_{\text{-Cy5.5}}$/FCS NPs, all at an equivalent $BSA_{\text{-Cy5.5}}$ dosage of 0.1 mg mL^{-1} for 4 h. Subsequently, the cells were examined using CLSM and flow cytometry to evaluate the uptake efficiency. As illustrated in Fig. 3a and b, the cells incubated with UM-15@$BSA_{\text{-Cy5.5}}$, or UM-15@$BSA_{\text{-Cy5.5}}$/FCS NPs exhibited significantly stronger $BSA_{\text{-Cy5.5}}$ fluorescence compared to those incubated with free $BSA_{\text{-Cy5.5}}$. This observation was further supported by the quantitative results obtained from

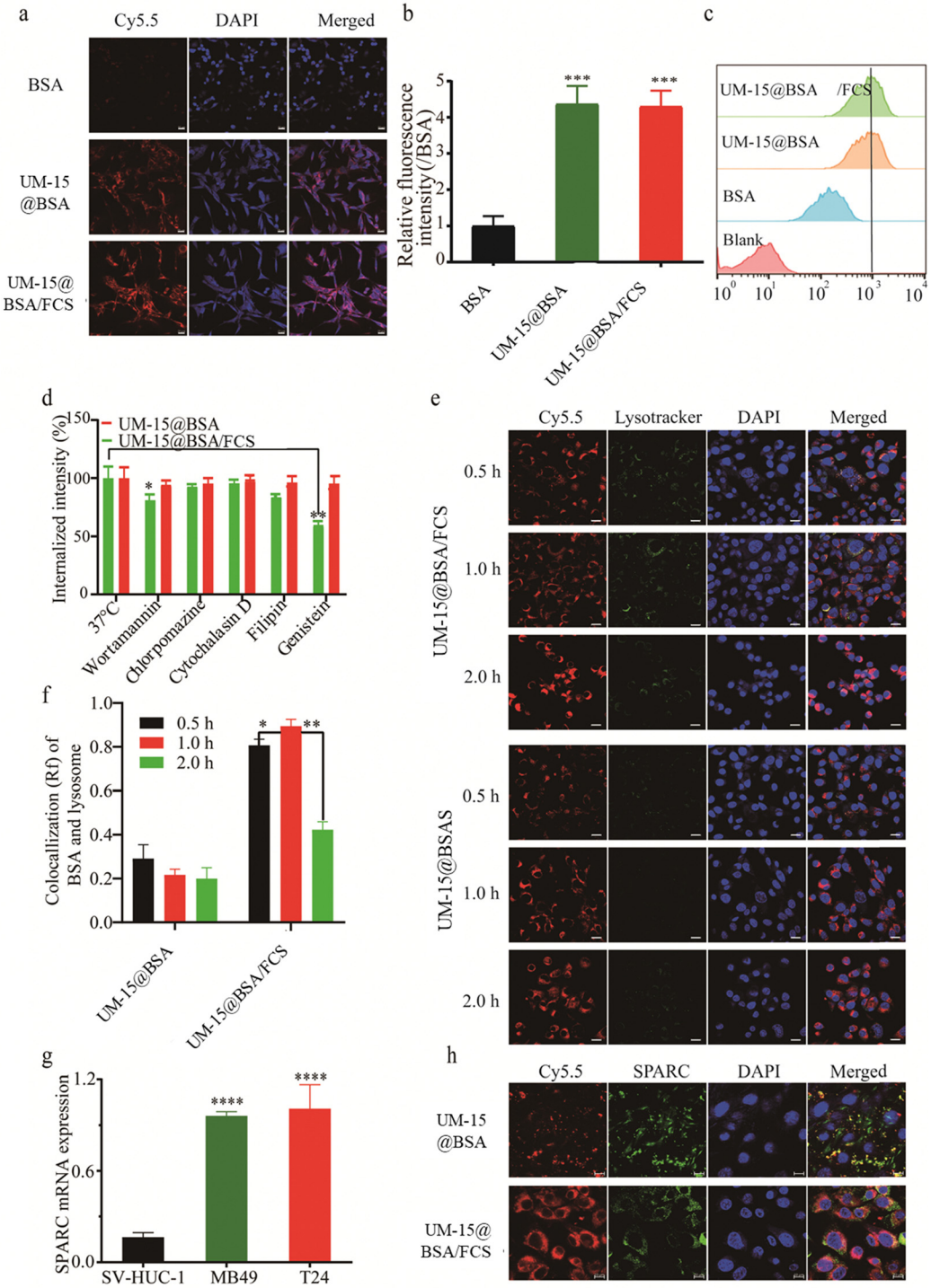

Fig. 3 The cell uptake and possible uptake pathway of UM-15@BSA and UM-15@BSA/FCS NPs. (a) Confocal images of MB49 cells after incubation with different BSA-based formulations for 4 h (scale bar 20 μm). (b) Semiquantitative analysis of the fluorescence intensity of $BSA_{-Cy5.5}$ based on the observations in (a) using ImageJ software. (c) The quantitative analysis of the cell uptake efficiency by fluorescence-activated cell sorting (FACS). (d) The cellular uptake of UM-15@BSA and UM-15@BSA/FCS NPs in MB49 cells pre-treated with various endocytosis inhibitors as indicated by flow cytometry. (e) Confocal fluorescence images to exhibit the intracellular trafficking of UM-15@BSA and UM-15@BSA/FCS NPs (scale bar 10 μm). (f) Semiquantitative analysis of colocalization between $BSA_{-Cy5.5}$ signals and LysoTracker signals in (d). (g) The evaluation of the mRNA expression of SPARC in MB49, T24, and SV-HUC-1 cells by Q-PCR. (h) The co-localization of BSA-cy5.5 signals and SPARC immunofluorescence in MB49 cells by CLSM (scale bar 10 μm). *$p < 0.05$, **$p < 0.01$, ***$p < 0.001$, and ****$p < 0.0001$ analyzed using Student's t test. Data are presented as mean ± standard deviation.

fluorescence-activated cell sorting (FACS), which depicted a notable increase in the cellular uptake efficiency of the NPs (Fig. 3c). These observations provide evidence that this nanostructure fabrication can greatly enhance the cellular uptake of BSA therapeutics.

Subsequently, the possible cellular uptake pathway of UM-15@BSA and UM-15@BSA/FCS NPs was explored by employing various endocytosis inhibitors, including wortmannin, chlorpromazine, cytochalasin D, genistein, and filipin. The results obtained from flow cytometry analysis demonstrated a distinct decrease in the cellular uptake of UM-15@BSA/FCS NPs in cells pre-treated with wortmannin (18.2 ± 2.8%), genistein (41.6 ± 2.4%), or filipin (16.9 ± 2.1%), indicating that the internalization of UM-15@BSA/FCS NPs mainly relied on a combination of micropinocytosis and caveolae-mediated pathways. In stark contrast, the uptake efficiency of UM-15@BSA for cells pre-incubated with those endocytosis inhibitors exhibited no significant change (Fig. 3d). Additionally, the investigation of intracellular trafficking through CLSM showed that, in comparison to the evident involvement of lysosome processes in the endocytosis of UM-15@BSA/FCS NPs, no significant lysosome signals were observed throughout the cellular uptake process of UM-15@BSA (Fig. 3e). The semi-quantitative analysis of the co-localization of $BSA_{-Cy5.5}$ signals and lysosome fluorescence, as depicted in Fig. 3f, further supports the absence of lysosomes in the cellular uptake process of UM-15@BSA, which is a characteristic of receptor-mediated cell transportation. These findings collectively indicate that the receptor-mediated endocytosis mechanism is likely involved in the cellular uptake of bare UM-15@BSA, rather than the micropinocytosis and caveolae-mediated conventional endocytosis pathways. Based on this deduction, we evaluated the SPARC expression in bladder cancer cells, which is the primary mechanism responsible for the uptake of albumin by several tumors.[29,30] As shown in Fig. 3g, MB49 and T24 bladder cancer cells demonstrated a high-level mRNA expression, significantly surpassing that of the human immortalized bladder epithelium SV-HUC-1 cells. In addition, obvious co-localization of $BSA_{-cy5.5}$ signals and SPARC immunofluorescence was observed in MB49 cells incubated with UM-15@BSA (Fig. 3h), which combined with the above results fully evidence that the potent uptake efficiency of bare UM-15@BSA is likely contributed to SPARC-mediated cell transportation.

Next, we investigated the mechanisms underlying UM-15-based intravesical therapy. Firstly, the *in vitro* cytotoxicity of different UM-15 loading formulations against bladder cancer T24 and MB49 cell lines, as well as SV-HUC-1cells, was determined by the CCK8 assay. It was found that BSA/FCS demonstrated minimal cytotoxicity against all types of cells (IC_{50} > 50 μM), suggesting the biosafety of this instillation carrier. Besides, in comparison to the non-selective cytotoxicity of free UM-15, both UM-15@BSA and UM-15@BSA/FCS NPs showed notable selective cytotoxicity against two types of bladder cancer cells, highlighting the specificity and effectiveness of UM-15@BSA therapeutics in targeting bladder cancer cells (Fig. S3a, ESI†). Combined with the aforementioned findings, it can be inferred that the SPARC-mediated tumor uptake and TEM-responsive drug release largely contributed to the selectivity and efficacy of the BSA loading therapeutics. Then, the *in vitro* induction of apoptosis and cell cycle arrest by different BSA based nanostructures was assessed using Annexin V-FITC/PI apoptosis staining and flow cytometry analysis. The results showed the significant effects of UM-15@BSA agents in promoting apoptosis and arresting the cell cycle (Fig. 4a, b and Fig. S3b, c, ESI†). The efficiency of BSA based formulations in suppressing the invasion and migration of BCa cells was estimated through Transwell and cell migration assays. It was observed that the invasion capacities of T24 and MB48 cells treated with UM-15@BSA or UM-15@BSA/FCS NPs were greatly suppressed (Fig. 4c and d). Consistently, the wound healing assay also revealed that both UM-15@BSA and UM-15@BSA/FCS NPs were more effective in inhibiting cancer cell migration compared to free UM-15 (Fig. 4e and Fig. S3d, ESI†). Thus, it was confirmed that UM-15 loading in BSA formulations is not only able to selectively kill cancer cells *via* apoptosis and cycle arresting pathways, but also efficiently inhibits their migration and invasion to prevent carcinogenic progression. Next, to evaluate the inhibitory effects of UM-15@BSA therapeutics on tumor stemness, BCa stem-like cells were isolated from PDX models constructed with MIBC tissue samples using magnetic activated cell sorting (MACS) and were then incubated with free UM-15, UM-15@BSA or UM-15@BSA/FCS NPs for 48 h, respectively. As depicted in Fig. 4f and g, the number of cell spheres (diameter >100 μm) of the UM-15@BSA/FCS NP group was much smaller than that of the UM-15@BSA group, the latter group also demonstrated a significant reduction in sphere formation compared to the free UM-15 group. Additionally, the expression of stem cell-related proteins such as CD 133, CD44 and ALDH1A1 in the above cells treated with UM-15@BSA or UM-15@BSA/FCS NPs was also significantly inhibited (Fig. S3e, ESI†). Furthermore, as depicted in Fig. 4h, the UM-15@BSA based therapeutics demonstrated efficient suppression of bladder carcinoma initiation in the limiting dilutions xenograft and serial transplantation assays. These results fully confirmed the remarkable stemness inhibition effect of the UM-15-loading formulations, thereby enhancing their potential efficacy for the elimination of BCa.

With encouraging results suggesting the cascaded delivery capacity of BSA/FCS carriers to realize the transepithelial tumor-selecting accumulation of toxic agents, we proceeded to assess the intravesical instillation safety of UM-15@BSA/FCS NPs. The *in vitro* hemolysis experiment suggested that the encapsulation of UM-15 within BSA and subsequent binding with FCS resulted in significant inhibition of hemolysis, in contrast to the dose-dependent prohemolytic effect of free UM-15 (Fig. 5a), proving that the fabrication of BSA/FCS nanostructures can effectively enhance the intravesical biosafety of UM-15. In addition, when mice were daily instilled with free UM-15, UM-15@BSA or UM-15@BSA/FCS NPs (UM-15 content 0.2 mg mL^{-1}, 100 μL) four times, the UM-15@BSA/FCS NP group did not show any significant body weight loss, in sharp contrast to the free UM-15 group (Fig. 5b). Then, the main organs (heart, liver, spleen, lungs, kidneys, and bladder) and blood samples were collected two days after the final administration to evaluate the organ injury and hepatic/renal function. As depicted in Fig. 5c, noticeable injury bleeding phenomena indicated by black arrows were observed in the

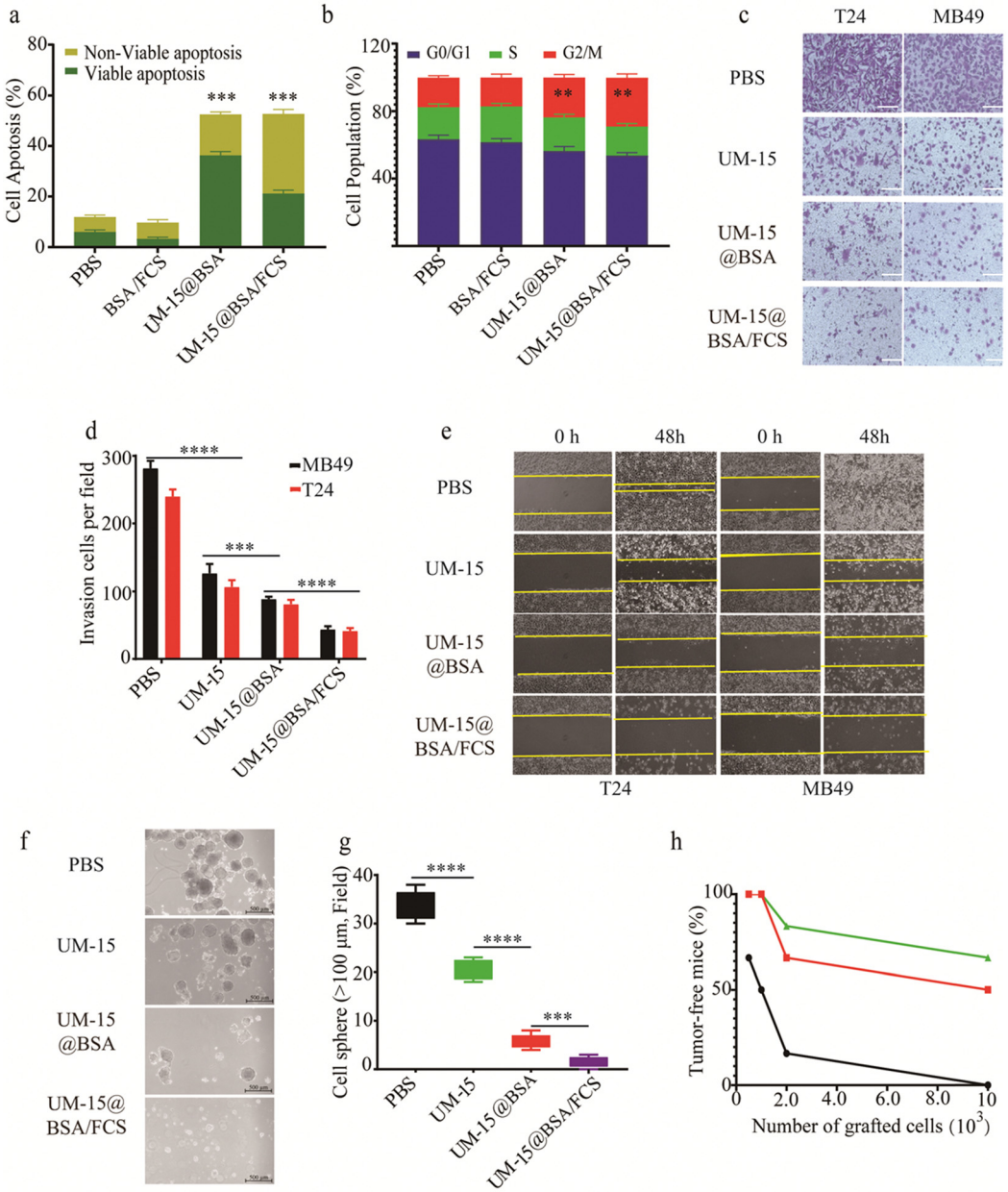

Fig. 4 The mechanisms underlying UM-15-based intravesical therapy. (a) The statistical data of the apoptotic rates of MB49 bladder cancer cells determined by Annexin V-FITC/PI co-staining and flow cytometry analysis. (b) The statistical data of the cell cycle of MB49 cells treated with different BSA-based formulations. (c) Transwell matrigel invasion assay measured changes in invasive ability (scale bar 200 μm) and (d) corresponding statistical analysis of the results from three independent experiments. (e) The wound-healing assay was used to measure the migration ability changes of MB49 cells treated with various UM-15 loading agents. (f) Representative image of sphere formation under a phase contrast microscope for BCa stem-like cells treated with UM-15 loading therapeutics (scale bar 500 μm) and (g) corresponding statistical analysis of the number of cell spheres was diameter >100 μm from three independent fields. (h) The suppression of bladder carcinoma initiation in the limiting dilutions xenograft and serial transplantation assays. $^{**}p < 0.01$, $^{***}p < 0.001$, and $^{****}p < 0.0001$ analyzed using Student's t test. Data are presented as mean ± standard deviation.

high magnification images of Haematoxylin–Eosin (H&E) stained sections of the spleens and kidneys of the UM-15 group. This observation suggests that the application of free UM-15 resulted in a certain degree of splenic and renal injuries, which may also be the reason for the subsequent unexpected early death of mice of the free UM-15 group during therapy. In remarkable contrast, no evident pathological abnormalities were recorded in the various organs of mice instilled with UM-15@BSA/FCS NPs. Moreover, the serum ALT/AST (liver function) and serum BUN levels (renal function) in mice treated with UM-15@BSA/FCS NPs also did not demonstrate abnormal fluctuations, in contrast to the significant increase in serum BUN levels observed in the free UM-15 group due to the renal damage ($P < 0.001$). Taken together, these findings provide strong evidence for the excellent tolerability and biosafety of BSA/FCS carriers, highlighting their essential role in facilitating the intravesical instillation of UM-15.

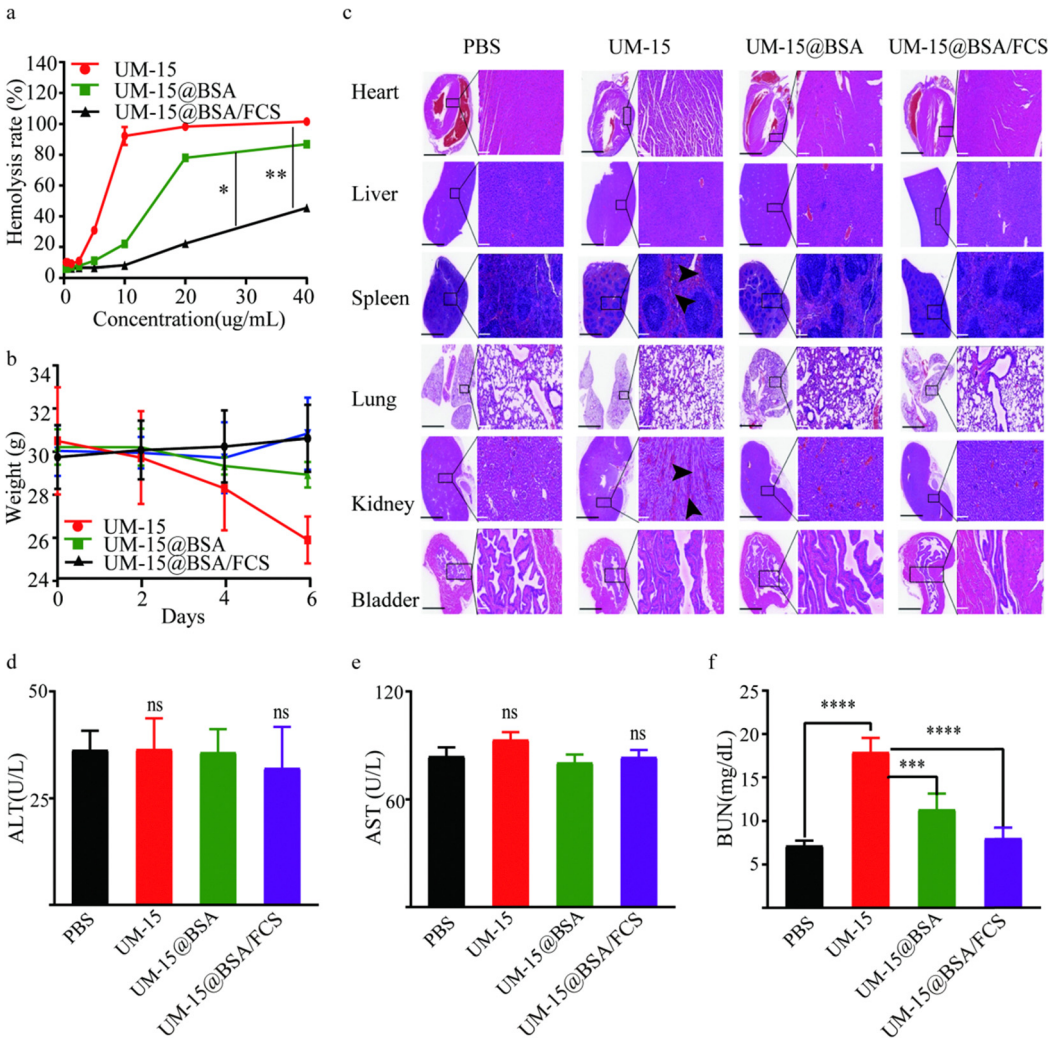

Fig. 5 Safety evaluation of intravesical instillation. (a) The *in vitro* hemolysis experiment for different UM-15 agents. (b) The body weight of mice in various groups after different treatments (n = 5). (c) The low (left, scale bar 1.25 mm) and high (right, scale bar 200 μm) magnification images of Haematoxylin–Eosin (H&E) stained sections of the six organs including heart, liver, bladder, spleen, lungs, and kidneys. (d) Hepatic function evaluated by ALT and AST levels and renal function by BUN levels in mice receiving various UM-15 agents (n = 5). *p < 0.05, **p < 0.01, ***p < 0.001, and ****p < 0.0001 analyzed using Student's t test. Data are presented as mean ± standard deviation.

Next, we investigated the therapeutic responses of UM-15@BSA/FCS NPs for BCa in an orthotopic BCa model at first. Mice with orthotopic bladder tumors were treated on day 7 (recorded as 0 day) after the injection of firefly-luciferase-expressing MB49 (fLuc-MB49) cells (recorded as −7 day) (Fig. 6a). The mice were divided into four groups (n = 6) and instilled with different types of agents weekly (PBS, free UM-15, UM-15@BSA, and UM-15@BSA/FCS NPs at a dose of UM-15 1.0 mg kg^{-1}). After four perfusion therapies, bioluminescence imaging and corresponding bioluminescence quantitative analysis suggested that the UM-15@BSA/FCS NP group showed the best tumor suppression effect among the four groups, as evidenced by the lowest tumor-specific bioluminescence signals (Fig. 6b and c) and a remarkably prolonged survival rate (Fig. 6d). Moreover, the weight of mice instilled with UM-15@BSA/FCS NPs remained stable throughout the treatment period (Fig. 6e). In contrast, the administration of free UM-15 or UM-15@BSA resulted in unexpected death and dramatic weight loss at the early stage of treatment, possibly due to the severe side effects and limited intravesical bioavailability of therapeutic agents. Therefore, the successful achievement of transepithelial tumor-selective cytotoxicity of UM-15@BSA/FCS NPs, combined with its tumor stemness inhibition, would contribute to the most effective therapy for BCa.

In addition to the proof-of-principle orthotopic MB49 BCa model, we further evaluated the therapeutic effect of UM-15@BSA/FCS NPs on a PDOX model, constructed by the tumor tissues obtained from an MIBC patient following the previously reported operation procedures in detail (Fig. 6f).[31,32] A treatment procedure was performed as depicted in Fig. 6f, and bladders were collected on day 28 to assess the final therapeutic effects of different UM-15-loading therapeutics. The results, as presented in Fig. 6g, demonstrated a significant reduction in the weight of the bladder with orthotopic tumors in the

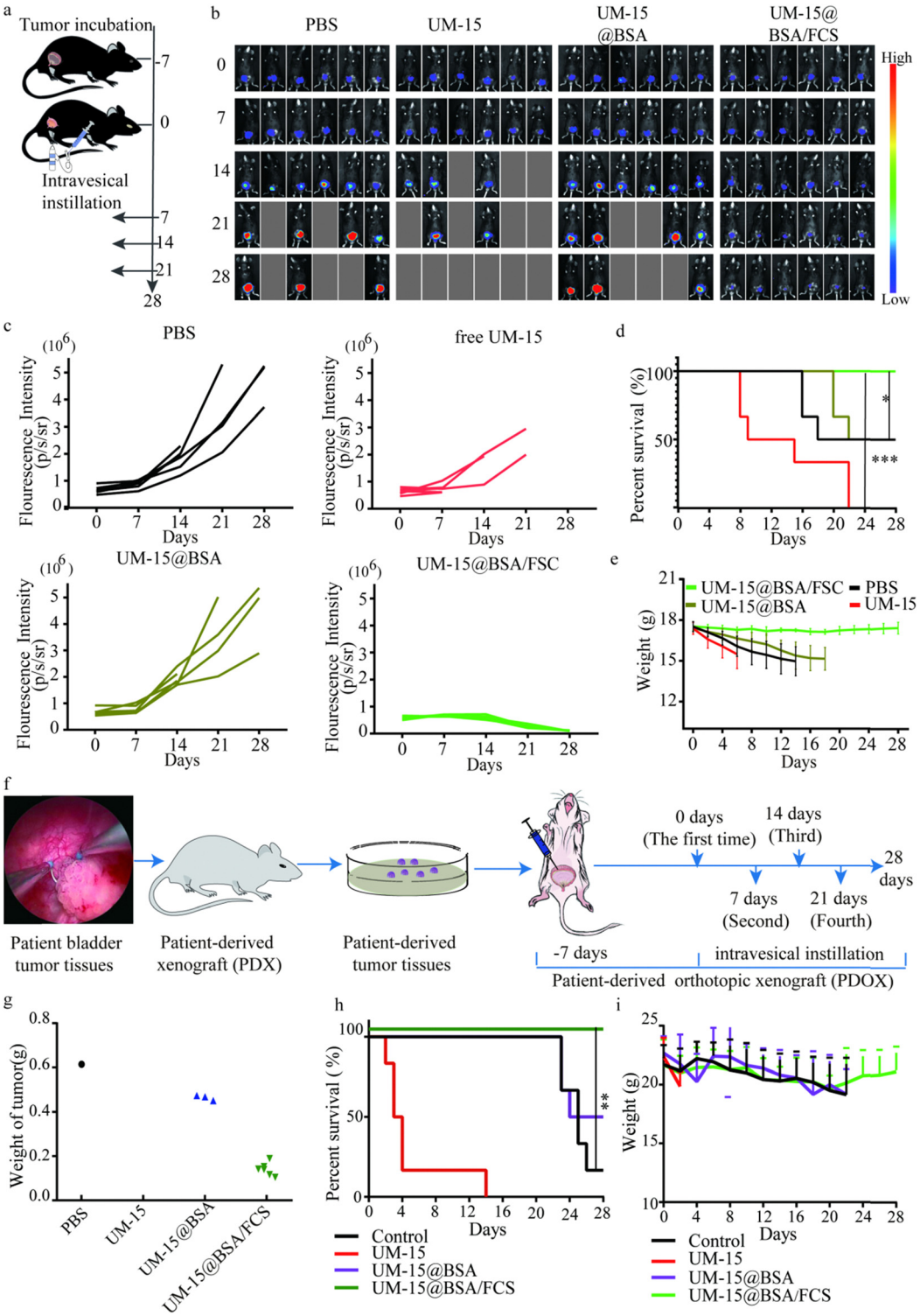

Fig. 6 Intravesical instillation to treat orthotopic BCa tumors. (a) Schematic illustration of intravesical instillation to inhibit orthotopic MB49 bladder tumors. (b) *In vivo* bioluminescence images to track the growth of tumor cells after various treatments. (c) The bioluminescence signal intensities of tumors during intravesical treatment. (d) Cumulative survival rate of mice in different groups. (e) Average body weights of mice within 28 days of treatment. (f) Schematic illustration of the construction of the PDOX model and the corresponding instillation treatment. (g) The weights of orthotopic bladder tumors collected from mice at the 28th day. (i) The body weights of mice within 28 days during the treatment. *$p < 0.05$, **$p < 0.01$, and ***$p < 0.001$, analyzed using Student's *t* test. Data are presented as mean ± standard deviation.

UM-15@BSA/FCS NP group compared to the other groups. Additionally, in contrast to the unexpected early death observed in the free UM-15 group, the UM-15@BSA/FCS NP group exhibited the longest survival time and normal weight fluctuations

(Fig. 6h and i), which were similar to those recorded in the orthotopic MB49 BCa model, providing further evidence of improved treatment outcomes and intravesical biosafety with the application of UM-15@BSA/FCS NPs.

Furthermore, we also verify the common applicability of BSA/FCS vehicles for other chemotherapy agents and compare the therapeutic effects of UM-15 with the first-line perfusion chemotherapeutics for BCa therapy. Gemcitabine (Gem), a clinical guidelines recommended chemotherapy drug for BCa, was selected as the control agent, and a GEM@BSA/FCS nanosystem was also prepared following a similar method to that described above. According to the treatment procedure shown in Fig. 6a, the chemotherapeutic efficacy of Gem (Gem, 0.8 mg kg^{-1}), Gem@BSA/FCS (Gem, 0.8 mg kg^{-1}) and UM-15@BSA/FCS (UM-15, 1.0 mg kg^{-1}) in the orthotopic MB49 BCa model was evaluated. As shown in Fig. S4a and b (ESI†), compared to mice instilled with PBS or free Gem, the tumor fluorescence for mice treated with Gem@BSA/FCS appeared to be much weaker. Combined with above mentioned significantly therapeutic outcome of UM-15@BSA/FCS, the therapeutic enhancement by the BSA/FCS vehicle on intravesical chemotherapeutics was reconfirmed, indicating the common applicability of BSA/FCS for chemotherapeutic drugs. Besides, mice treated with UM-15@BSA/FCS showed a more remarkably tumor inhibition effect compared with that of the Gem@BSA/FCS group, suggesting the advantage of UM-15 in BCa therapy.

Conclusion

In the present study, UM-15 is synthesized and recognized as a potentially effective chemotherapeutic agent for BCa therapy due to its potent cytotoxicity and ability to inhibit BCa stemness. To facilitate the intravesical application of UM-15, FCS-binding albumin carriers were fabricated using a green method involving the hydrogen bonding or van der Waals force-mediated assembly of BSA through thermal annealing operation and subsequent electrostatic interaction between UM-15@BSA and FCS. The coating of FCS on the albumin system was mainly responsible for the transepithelial delivery of intravesical UM-15@BSA to the bladder through reversible regulation in tight junctions of the bladder epithelium. Subsequently, the FCS-albumin complexes would dissociate into bare UM-15@BSA nanostructures owing to the charge repulsion, which is triggered by the charge reversal effect of UM-15@BSA in response to the tumor microenvironment (pH 6.5–6.8). Consequently, due to the smaller size advantage, the bare UM-15@BSA formulations are able to penetrate more effectively into the tumor tissue and demonstrate remarkably enhanced tumor selectivity *via* the SPARC pathway-mediated tumor uptake and disulfide bond-driven GSH-responsive drug release. Ultimately, the incorporation of UM-15 into the nanovehicle leads to remarkable enhancements in the efficacy of intravesical treatments in both mouse orthotopic and orthotopic PDX bladder tumor models, while also mitigating adverse effects. Thus, this work presents a new therapeutic agent for bladder cancer therapy and proposes an economical and convenient approach to develop a smart transepithelial drug delivery system for the targeted delivery of therapeutics to bladder tumors *via* an intravesical cascade delivery mechanism.

Experimental section

Chemicals and materials

The main reagents for the synthesis of UM-15 such as phloroglucinol, ethyl diacetoacetate, phosphorus(v) oxychloride ($POCl_3$), nerol, phosphorus tribromide (PBr_3), and pyridine were all purchased from Aladdin Biochemical Technology Co., Ltd (Shanghai, China). Chitosan (DD% $\geq$95%), perfluoroheptanoic acid, *N*-hydroxysuccinimide (NHS), and *N*-(3-dimethylaminopropyl)-*N*-ethylcarbodiimide hydrochloride crystals (EDC) were supplied by JK Chemical Company (Beijing, China). Bovine serum albumin (BSA) and cell culture related reagents were purchased from Life Technologies Co. (New York, USA). The cell cycle and apoptosis analysis kit, and Anti-CD133, Anti-CD44, and ALDH1A1 antibodies were obtained from Abcam (Cambridge, USA). Primers were synthesized by Sangon Bioengineering Co., Ltd (Shanghai, China). All chemical reagents employed in this work were of analytical grade.

Cell lines and mice

A commercially available luciferase lentivirus transfection kit (Shanghai Genechem Co., Ltd) was employed to prepare fLuc-MB49 and fLuc-T24 cells. Female C57 bl mice, SCID mice, and balb/c nude mice that are 10-12 weeks old were provided by GemPharmatech Co., Ltd (Guangdong, China) and employed following protocols approved by the Model Disease Animal Center of Shenzhen Institute of Precision Medicine (ECPM-2023010254). Tumor tissues of MIBC patients were collected from the Institute of Urology of Afffliated Luohu Hospital of Shenzhen University and approved by the Medical Ethics Committee of the Affiliated Luohu Hospital of Shenzhen University (2020-LHQRMYY-KYLL-007).

Synthesis of FCS

FCS was synthesized by our previously reported method.[33] Generally, perfluoroheptanoic acid (55.0 μM, 156 mg) was mixed with EDC (82.5 μM, 200 mg) and NHS 82.5 μM, 94.86 mg) under stirring in the dark at room temperature for 0.5 h, which were then added into the 1% acetic acid solution of chitosan for stirring in the dark for 24 h. Then a dialysis bag (MWCO 3500 Da, Technologies Co.) was employed for purification in double-distilled water for 48 h. The samples were lyophilized and identified by ninhydrin colorimetry and ^{19}F NMR (Bruker AV III 600 spectrometers) spectroscopy as previously reported by us.[33,34]

Synthesis of UM-15@BSA NPs

The former was prepared by a mild thermal annealing method.[35] Briefly, a 200 μL DMF solution of UM-15 was added dropwise into 1.0 mL of BSA solution (10.0 mg mL^{-1}) under vortexing. Then, the mixture was incubated at 70 °C for 40 min,

and sequentially cooled to room temperature. The thus-formed NPs (denoted as UM-15@BSA NPs) were purified by centrifugation at 14 800 rpm for 5 min to remove BSA aggregations and insoluble UM-15 and then a dialysis bag (MWCO 3500 Da) was used to remove DMF.

Preparation of FCS binding albumin NPs

UM-15@BSA/FCS NPs were prepared using a self-assembly approach. Generally, the solution of FCS was mixed with UM-15@BSA at various weight ratios (1 : 4–2 : 1) for 2 h. The obtained UM-15@BSA/FCS NPs were purified using a Sephadex G50 column (GE Healthcare, USA).

Detection of the CD spectrum and ITC

The CD spectrum was recorded using a circular dichroism spectrometer with a light diameter of 1 mm, a measurement temperature of 295 K, and a recording range of 190–260 nm. The concentration of BSA used to determine the CD spectrum was 1.5×10^{-6} M. A NANO-ITC isothermal titration microcalorimeter was used in the ITC experiment. The sample pool volume was 300 μL and the syringe volume was 50 μL. 300 μL (20 μmol L^{-1}) of BSA solutions was injected into the sample pool, and 50 μL (230 μmol L^{-1}) of UM-15 solution was injected into the syringe, kept at a constant temperature of 298 K, and titrated after the baseline was stabilized. The titration volume was 2 μL each time, and the interval was 120 s. PBS containing 5% DMSO was applied as a control solution. The calorimetric curve was obtained after titration, and the thermodynamic parameters such as enthalpy change (ΔH), entropy change (ΔS) and dissociation constant (K_d) were then obtained.

Nanoparticle characterization

A Thermo Scientific LTQ-Orbitrap XL (Thermo Scientific, Bremen, Germany) was used to record the high-resolution electrospray ionization mass spectrum (HR-ESI-MS) of UM-15. ^{13}C and ^{1}H nuclear magnetic resonance (NMR) spectra of UM-15 were collected using a Bruker AV III 600 spectrometer (TMS as the internal reference). These FCS binding albumin NPs were analyzed using a Zetasizer Lab (Malvern, UK) to record the size and ζ-potential. UV absorbance spectra of different agents were detected *via* an ultraviolet-visible-NIR spectrophotometer (PerkinElmer Lambda 750, USA). Transmission electron microscopy (TEM, FEI Tecnai F20, acceleration voltage = 200 kV) was employed to investigate the morphology of these NPs. The drug-loading (DL) capacity and encapsulation efficiency (EE) were calculated following the classical formula.[36]

Freeze-drying stability of nanoparticles

The size changes and UM-15 content fluctuations between NP PBS solution and its redissolved alternatives were monitored by the dynamic light scattering technique and high performance liquid chromatography (HPLC), respectively.

In vitro drug release

The release profile of UM-15 from the UM-15@BSA/FCS NPs was investigated carefully. Briefly, 1 mL of UM-15@BSA/FCS NPs (10 mg mL^{-1}, 1.89 mg mL^{-1} UM-15) was placed in a dialysis bag (MWCO 8 kDa) and then immersed in 20 mL of PBS containing 0.5% w/v SDS (pH 7.4, pH 5.5, 5.0 Mm GSH, pH 5.5 + 5.0 mM GSH). The experiment was performed at 37 °C with continuous stirring at 110 rpm. At predetermined time intervals, aliquots of dialysate (0.5 mL) were collected for measurement and replenished with an equal volume of fresh pre-processed medium. The released amount of UM-15 was determined by HPLC.

Cell culture

Human bladder cancer T24 and murine bladder cancer MB49 cells were incubated in RPMI-1640 medium and Dulbecco's modified Eagle's medium, respectively. Human bladder epithelium immortalized SV-HUC-1 cells were maintained in Ham's F12 medium. All these cells were cultured with complete medium containing 10% FBS and 1% antibiotics at 37 °C under a humidified atmosphere and 5% CO_2.

In vitro cellular uptake

MB49 cells were seeded on a 12-well plate at a density of 1.0×10^5 cells per well and then incubated with various Cy5.5-labeled BSA agents (BSA-Cy5.5 concentration: 10 μg mL^{-1}) for 4 h. Subsequently, the cells were fixed with 4% paraformaldehyde and counterstained with DAPI. Fluorescence images were recorded using confocal laser scanning microscopy (CLSM, Zeiss LSM 510, Germany). In addition, the quantitative analysis of the above cellular uptake was performed by flow cytometry (BD FACSCalibur).

Intracellular trafficking

To clarify the intracellular trafficking of UM-15@BSA and UM-15@BSA/FCS NPs, cells were incubated with these NPs for different times (0.5, 1.0, and 2.0 h), respectively. Then, the cells were maintained with LysoTracker (50 nM, Thermo Fisher Scientific) for 1 h, and subsequently counterstained with DAPI for CLSM imaging.

Endocytosis inhibition

Various endocytosis inhibitors were applied to investigate the possible endocytosis mechanism of UM-15@BSA and UM-15@BSA/FCS NPs. MB49 cells were seeded on a 12-well plate at a density of 2.0×10^5 cells per well and then various inhibitors including wortmannin (0.021 μg mL^{-1}, Sigma), chlorpromazine (10 μg mL^{-1}, Sangon Biotech), cytochalasin D (5 μg mL^{-1}, Sangon Biotech), filipin (5 μg mL^{-1}, Sigma), or genistein (54 μg mL^{-1}, Sangon Biotech) were added individually for 1 h incubation. Then, the solution containing inhibitors was replaced by UM-15@BSA or UM-15@BSA/FCS NPs containing the same inhibitors and maintained for another 1 h for flow cytometry analysis. The colocalization of BSA and lysosome was semi-quantitatively analyzed using ImageJ software.

RT-PCR for the determination of the mRNA expression of SPARC

Quantitative real-time RT-PCR was employed to evaluate the expression of SPARC on MB49, T24, and SV-HUC-1 cells.

An RNeasy Plus Mini Kit (Qiagen), a QuantiTect reverse transcription kit (Qiagen), and an SYBR Green Core Reagent Kit (Qiagen) were used following the reported manufacturer's instructions. PCR primer sequences were as follows: Sparc (*Mus musculus*), 5′-TTCAGACCGCCAGAACTCTT-3′ (forward) and 5′-CACGGT TTCCTCCTCCAC TA-3′ (reverse); SPARC (*Homo sapiens*), 5′-GTGCAGAGG AAACCGAAGAG-3′ (forward) and 5′-AAGTGGCAGGAAGAGTCGAA-3′ (reverse). Eventually, the efficiency-corrected ΔCT approach: quantity = (efficiency + 1) − CT was used to estimate the mRNA expressions of SPARC following previously described protocols.[37,38]

In vitro cytotoxicity

The cytotoxicity of free UM-15, UM-15@BSA, and UM-15@BSA/FCS NPs against T24, MB49, and SV-HUC-1 cells denoted as half maximal inhibitory concentration (IC_{50}) was determined by the CCK-8 assay following the vendor's protocol. Besides, the apoptosis induced by different UM-15 agents was measured using an Annexin V-FITC/PI apoptosis detection kit (Beyotime, China) according to the manufacturer's protocol. MB49 cells were pretreated under a similar process and eventually analyzed by FACS. Furthermore, the MB49 cell cycle arrest was also quantitatively detected by FACS. Briefly, MB49 cells in the logarithmic growth phase were incubated with different UM-15 agents (UM-15, 5.0 μg mL^{-1}), which were collected after 24 h of incubation and then maintained with 70% ethanol overnight. Subsequently, the cells were stained with PI at 4 °C for 0.5 h and applied for the measurement of the cell cycle phase distribution by FACS.

In vitro invasion and migration assays

MB49 cells were seeded on a 6-well plate at a density of 1.0×10^6 cells per well to form a dense distribution. After 48 h of incubation, an artificial wound was created and fresh medium containing different UM-15 agents (UM-15, 5.0 μg mL^{-1}) were added. To monitor migration-induced wound healing, images were taken at 0 and 48 h. For the Transwell invasion assay, 3×10^4 MB49 cells were seeded in the top chamber with serum-free medium (24-well insert; 8 μm; Corning). As a chemoattractant, medium containing 10% serum was loaded in the lower chamber. After 24 h of incubation, the non-migrated cells in the upper chamber were removed using a cotton swab, and the filters were individually stained with 2% crystal violet. Then, the invasive cells were captured using a light microscope.

Cell sphere formation

MB49 cells incubated with different UM-15 agents for 48 h were seeded in ultra-low attachment 6-well plates (Corning Inc., USA) at a density of 5.0×10^3 cells per well. Then the cells were maintained in specific medium as previously reported, and the spheres whose diameter exceeded 200 μm were counted. The cell sphere formation efficiency was calculated as (number of spheres formed/field).

Hemolytic assay

Red blood cells (RBCs) were collected from Sprague Dawley rats according to the approach previously reported.[39] The RBC suspension (0.2 mL, 3.0×10^3 cells per mL) was mixed with free UM-15, UM-15@BSA, or UM-15@BSA/FCS NPs at different UM-15 concentrations (10–40 μg mL^{-1}). The following operations, optical density measurement, and percent hemolysis calculation were carried out according to the previous reference.[40]

The transepithelial capacity of UM-15@BSA/FCS NPs

To estimate the transepithelial penetration capacity of these BSA-based formulations, a frozen section experiment was performed as previously described by us. In brief, mice were intravesically instilled with free BSA, UM-15@BSA, or UM-15@BSA/FCS NPs for 1 h. Then bladders were collected for fluorescence distribution analysis using CLSM. The semi-quantitative analysis of the fluorescence intensity and penetration depth was performed using ImageJ software.

Immunofluorescence

SV-HUC-1 cells (4.0×10^5 cells per mL) were seeded on the round coverslips in 12-well plates for 48 h of incubation to form a dense cell layer. Then, different BSA agents were added and maintained for 1 h. Subsequently, the cells were incubated with tight junction protein-related antibodies including ZO-1 (1 : 150, Abcam, USA), occludin (1 : 100, Abcam, USA), MLC (1 : 100, Abcam, USA), and pMLC (1 : 100, Abcam, USA), and imaged by CLSM following our previously reported protocol.[33]

In vivo toxicity of UM-15@BSA/FCS NPs

To evaluate the instillation safety of UM-15@BSA/FCS NPs, blood samples and main organs of healthy female C57 bl mice instilled with deionized water or various UM-15 agents (1.0 mg kg^{-1} UM-15 containing) daily were collected and analyzed on day 2 after the last injection. After intravesical instillation 4 times, the weights recorded every other day, the levels of ALT, AST, and BUN in blood samples, and H&E staining of six main organs (heart, liver, spleen, lungs, kidneys, and bladder) were analyzed.

Therapeutic efficacy of UM-15@BSA/FCS NPs

The orthotopic MB49 BCa model of female C57 bl mice and the patient-derived orthotopic xenograft model were constructed following our well documented approaches. For intravesical therapy, 100 μL of deionized water, free UM-15, UM-15@BSA, or UM-15@BSA/FCS NPs (UM-15, 1.0 mg kg^{-1}) solution was administered through a closed IV catheter system (0.7 mm × 19 mm, BD Intima II) for 1 h. Mice were treated weekly and weighed every other day. Eventually, bladders with tumors were collected and analyzed on day 7 after the fourth treatment. For the orthotopic MB49 BCa model, an IVIS Lumina system (Caliper Life Sciences) was used to record the growth of orthotopic tumors.

In situ tumor formation assay

fLuc-T24 cells incubated with UM-15@BSA or UM-15@BSA/FCS NPs for 48 h were injected into the bladder wall of female C57 bl mice in a series of cell numbers (500, 1000, 2000, and 10 000).

The bioluminescence was recorded using an IVIS Lumina system weekly and the percentage of tumor-free mice within two months was calculated.

Statistical analysis

All experimental data are presented as mean ± SD. All quantitative and semiquantitative results were entered in GraphPad Prism 8.0.1 to perform statistical analysis. Student's *t*-test and one-way ANOVA were used for data analysis. All experiments were repeated at least three times.

Author contributions

Y. L. and D. D. contributed equally and are co-first authors for this work. G. L. conceived the project. G. L. and Y. L. wrote the manuscript. Y. L., D. D., Q. L., S. Y., and X. L. carried out the experiments. D. D. completed the data analysis. G. L. supervised the whole work.

Data availability

All data included in this study are available upon request by contacting the corresponding author.

Conflicts of interest

The authors declare that they have no known competing financial interests or personal relationships that could have appeared to influence the work reported in this paper.

Acknowledgements

This work was partially supported by the National Natural Science Foundation of China (82003620 and 82102979), the National Natural Science Foundation of China (92359202), the Medical Scientific Research Foundation of Guangdong Province (A2022024), the Natural Science Foundation of Guangdong Province (2022A1515012003), the Shenzhen Scientific and Technological Research Program (JSGG20201103153801005), and the Guangdong Basic and Applied Basic Research Foundation (2021A1515110402).

References

1 A. Richters, K. Aben and L. K. J. S. B. Heidelberg, The global burden of urinary bladder cancer: an update, *World J. Urol.*, 2020, **38**(8), 1895–1904.
2 J. Zhu, Z. Tian, Y. Li, X. Hua and C. J. A. S. Huang, ATG7 Promotes Bladder Cancer Invasion *via* Autophagy-Mediated Increased ARHGDIB mRNA Stability, *Adv. Sci.*, 2019, **6**(8), 1801927.
3 W. Jing, C. Chen, G. Wang, M. Han, S. Chen, X. Jiang, C. Shi, P. Sun, Z. Yang, B. Shi and X. Jiang, Metabolic Modulation of Intracellular Ammonia *via* Intravesical Instillation of Nanoporter-Encased Hydrogel Eradicates Bladder Carcinoma, *Adv. Sci.*, 2023, **10**(12), e2206893.
4 S. Maclennan, E. Duncan, T. Skolarus, M. Roobol, V. Kasivisvanathan, K. Gallagher, G. Gandaglia, V. Sakalis, E. Smith and K. J. E. u f Plass, Improving Guideline Adherence in Urology, *Eur. Urol. Focus*, 2021, **8**(5), 1545–1552.
5 J. A. Witjes, H. M. M. Bruins, R. L. Cathomas, V. M. Compérat and A. G. V. D. J. E. U. Heijden, European Association of Urology Guidelines on Muscle-invasive and Metastatic Bladder Cancer: Summary of the 2020 Guidelines, *Eur. Urol.*, 2020, **79**(1), 82–104.
6 G. Li, Q. Lei, F. Wang, D. Deng, S. Wang, L. Tian, W. Shen, Y. Cheng, Z. Liu and S. J. S. Wu, Fluorinated Polymer Mediated Transmucosal Peptide Delivery for Intravesical Instillation Therapy of Bladder Cancer, *Small*, 2019, **15**(25), e1900936.
7 Z. Yang, C. Li, H. Liu, X. Zhang and S. J. E. U. Wu, Single-cell Sequencing Reveals Variants in ARID1A, GPRC5A and MLL2 Driving Self-renewal of Human Bladder Cancer Stem Cells, *Eur. Urol.*, 2017, **71**(1), 8–12.
8 A. O. Elzoghby, W. M. Samy and N. A. J. J. o C. R. Elgindy, Albumin-based nanoparticles as potential controlled release drug delivery systems, *J. Controlled Release*, 2012, **157**(2), 168–182.
9 M. Rahman, K. Alam, A. Hafeez, R. Ilyas and S. J. N. S. f C. T. Beg, Protein-based nanomedicines as anticancer drug delivery platforms, *Nanoformulation Strategies Cancer Treat.*, 2021, 153–169.
10 T. Lin, P. Zhao, Y. Jiang, Y. Tang, H. Jin, Z. Pan, H. He, V. C. Yang and Y. Huang, Blood Brain-Barrier-Penetrating Albumin Nanoparticles for Biomimetic Drug Delivery *via* Albumin-Binding Protein Pathways for Antiglioma Therapy, *ACS Nano*, 2016, **231**, 9999–10012.
11 V. D. Jaiswal, D. S. Pangam and P. M. Dongre, Biophysical study of cisplatin loaded albumin-gold nanoparticle and its interaction with glycans of gp60 receptor, *Int. J. Biol. Macromol.*, 2023, **231**, 123368.
12 I. Hassanin and A. Elzoghby, Albumin-based nanoparticles: a promising strategy to overcome cancer drug resistance, *Cancer Drug Resist.*, 2020, **3**(4), 930–946.
13 Z. He, K. Chen, Y. An, J. He, X. Zhang, L. Tang, F. Sun and K. Jiang, BSA modification of bacterial surface: a promising anti-cancer therapeutic strategy, *BMC Microbiol.*, 2023, **23**(1), 105.
14 J. Larson, T. Yasmin, D. A. Sens, X. D. Zhou, M. A. Sens, S. H. Garrett, J. R. Dunlevy, L. Cao and S. Somji, SPARC gene expression is repressed in human urothelial cells (UROtsa) exposed to or malignantly transformed by cadmium or arsenite, *Toxicol. Lett.*, 2010, **199**(2), 166–172.
15 J. Lv, C. Wang, H. Li, Z. Li, Q. Fan, Y. Zhang, Y. Li, H. Wang and Y. Cheng, Bifunctional and Bioreducible Dendrimer Bearing a Fluoroalkyl Tail for Efficient Protein Delivery Both In Vitro and In Vivo, *Nano Lett.*, 2020, **20**(12), 8600–8607.
16 G. Rong, C. Wang, L. Chen, Y. Yan and Y. Cheng, Fluoroalkylation promotes cytosolic peptide delivery, *Sci. Adv.*, 2020, **6**(33), eaaz1774.

17 H. Wang, Y. Xie, Y. Chen, H. Zhao, X. Lv, Z. Zhang, G. Li, J. Pan, J. Wang and Z. Liu, Transdermal Delivery of Photosensitizer-Catalase Conjugate by Fluorinated Polyethylenimine for Enhanced Topical Photodynamic Therapy of Bacterial Infections, *Adv. Healthcare Mater.*, 2023, **12**(26), e2300848.

18 J. Xin, X. Lu, J. Cao, W. Wu, Q. Liu, D. Wang, X. Zhou and D. Ding, Fluorinated Organic Polymers for Cancer Drug Delivery, *Adv. Mater.*, 2024, e2404645.

19 J. Lv and Y. Cheng, Fluoropolymers in biomedical applications: state-of-the-art and future perspectives, *Chem. Soc. Rev.*, 2021, **50**(9), 5435–5467.

20 Z. Zhang, W. Shen, J. Ling, Y. Yan, J. Hu and Y. Cheng, The fluorination effect of fluoroamphiphiles in cytosolic protein delivery, *Nat. Commun.*, 2018, **9**(1), 1377.

21 J. Lv, B. He, J. Yu, Y. Wang, C. Wang, S. Zhang, H. Wang, J. Hu, Q. Zhang and Y. Cheng, Fluoropolymers for intracellular and in vivo protein delivery, *Biomaterials*, 2018, **182**, 167–175.

22 G. Li, S. Wang, D. Deng, Z. Xiao, Z. Dong, Z. Wang, Q. Lei, S. Gao, G. Huang, E. Zhang, G. Zeng, Z. Wen, S. Wu and Z. Liu, Fluorinated Chitosan To Enhance Transmucosal Delivery of Sonosensitizer-Conjugated Catalase for Sonodynamic Bladder Cancer Treatment Post-intravesical Instillation, *ACS Nano*, 2020, **14**(2), 1586–1599.

23 Q. Zhuang, T. Chao, Y. Wu, T. Wei, J. Ren, Z. Cao, R. Peng and Z. Liu, Fluorocarbon Modified Chitosan to Enable Transdermal Immunotherapy for Melanoma Treatment, *Small*, 2023, e2303634.

24 R. Sun, X. Li, G. Wang, H. Luo, Y. Huang, G. Wang, X. Zeng, G. Liu, Z. Wu and J. Song, Photoactivated H-2 Nanogenerator for Enhanced Chemotherapy of Bladder Cancer, *ACS Nano*, 2020, **14**(7), 8135–8148.

25 G. Li, X. Li, L. Cao, L. Zhang, L. Shen, J. Zhu, J. Wang and J. Si, Sesquiterpene coumarins from seeds of Ferula sinkiangensis, *Fitoterapia*, 2015, **103**, 222–226.

26 S. Y. Lee, S. Kim, J. Y. Tyler, K. Park and J. X. Cheng, Blood-stable, tumor-adaptable disulfide bonded mPEG-(Cys)4-PDLLA micelles for chemotherapy, *Biomaterials*, 2013, **34**(2), 552–561.

27 Z. Y. Qiao, R. Zhang, F. S. Du, D. H. Liang and Z. C. Li, Multi-responsive nanogels containing motifs of ortho ester, oligo(ethylene glycol) and disulfide linkage as carriers of hydrophobic anti-cancer drugs, *J. Controlled Release*, 2011, **152**(1), 57–66.

28 N. Zhang, F. Zhao, Q. Zou, Y. Li, G. Ma and X. Yan, Multitriggered Tumor-Responsive Drug Delivery Vehicles Based on Protein and Polypeptide Coassembly for Enhanced Photodynamic Tumor Ablation, *Small*, 2016, **12**(43), 5936–5943.

29 H. Lu, L. Noorani, Y. Jiang, A. W. Du and M. H. J. J. o M. C. B. Stenzel, Penetration and drug delivery of albumin nanoparticles into pancreatic multicellular tumor spheroids, *J. Mater. Chem. B*, 2017, **5**(48), 9591–9599.

30 L. Cheng, M. M. Niu, T. Yan, Z. Ma and C. J. A. P. S. B. Li, Bioresponsive micro-to-nano albumin-based systems for targeted drug delivery against complex fungal infections, *Acta Pharm. Sin. B*, 2021, **11**(10), 3220–3230.

31 G. Li, T. Tao, D. Deng, S. Zhang, Y. Chao, Y. Dai, Y. Li, R. Tao, S. Yuan and Z. J. B. Liu, Collagen-targeted tumor-specific transepithelial penetration enhancer mediated intravesical chemoimmunotherapy for non-muscle-invasive bladder cancer, *Biomaterials*, 2022, **283**, 121422.

32 K. Miyake, T. Kiyuna, M. Miyake, K. Kawaguchi, Z. Zhang, S. Wangsiricharoen, S. Razmjooei, H. Oshiro, T. Higuchi, Y. Li, S. Nelson, T. Murakami, Y. Hiroshima, T. Kumamoto, R. Matsuyama, M. Bouvet, S. R. Singh, S. Chawla, I. Endo and R. Hoffman, Gemcitabine combined with docetaxel precisely regressed a recurrent leiomyosarcoma peritoneal metastasis in a patient-derived orthotopic xenograft (PDOX) model, *Biochem. Biophys. Res. Commun.*, 2019, **509**(4), 1041–1046.

33 G. Li, S. Wang, D. Deng, Z. Xiao, Z. Dong, Z. Wang, Q. Lei, S. Gao, G. Huang, E. Zhang, G. Zeng, Z. Wen, S. Wu and Z. Liu, Fluorinated Chitosan To Enhance Transmucosal Delivery of Sonosensitizer-Conjugated Catalase for Sonodynamic Bladder Cancer Treatment Post-intravesical Instillation, *ACS Nano*, 2020, **14**(2), 1586–1599.

34 H. Song, W. U. Yue-Na and L. J. C. J. o I. o T. C. M. Mei, Quantitative Determination of Total Free-Amino Acid in Nervilia fordii(Hance) Schltr, *Ninhydrin Colorim. Method*, 2010, **53**(7), 1849–1859.

35 A. Yurij and Z. Irina, Macromolecules, Macromolecular complexes of BSA with gelatin, *Int. J. Biol. Macromol.*, 2012, **51**(3), 319–328.

36 C. X. Guo, J. Xie, H. Yang and C. M. J. A. S. Li, Au@CdS Core–Shell Nanoparticles-Modified ZnO Nanowires Photoanode for Efficient Photoelectrochemical Water Splitting, *Adv. Sci.*, 2015, **2**(12), 1500135.

37 M. A. Wood and W. H. Walker, USF1/2 transcription factor DNA-binding activity is induced during rat Sertoli cell differentiation, *Biol. Reprod.*, 2009, **80**(1), 24–33.

38 B. Hoang, M. Ernsting, A. Roy, M. Murakami, E. Undzys and S. Li, Docetaxel-carboxymethylcellulose nanoparticles target cells *via* a SPARC and albumin dependent mechanism, *Biomaterials*, 2015, **59**, 66–76.

39 K. Zhang, X. Xiao, L. Li, Y. Fan and X. Li, Development of novel oxygen carriers by coupling hemoglobin to functionalized multiwall carbon nanotubes, *J. Mater. Chem. B*, 2019, **7**(31), 4821–4832.

40 C. Gulmez, C. Altinkaynak, M. Turk, N. Ozdemir and O. J. C. Atakisi, Biodiversity, Hemoglobin-Inorganic Hybrid Nanoflowers with Different Metal Ions as Potential Oxygen Carrying Systems, *Chem. Biodivers.*, 2022, **19**(1), e202100683.